



Article

Dual-Responsive Nanotubes Assembled by Amphiphilic Dendrimers: Controlled Release and Crosslinking

Minghui Zhang ^{1,2} , Hui Yang ^{1,*} , Jiazhong Wu ³, Siyu Yang ³, Danfeng Yu ⁴, Xu Wu ⁴, Aiqing Ma ⁵, Keji Sun ⁵ and Jinben Wang ¹

¹ CAS Key Lab of Colloid, Interface and Chemical Thermodynamics, Institute of Chemistry, Chinese Academy of Sciences, Beijing 100190, China; zhangminghui@iccas.ac.cn (M.Z.); jbwang@iccas.ac.cn (J.W.)

² University of Chinese Academy of Sciences, Beijing 100049, China

³ State Key Laboratory of Enhanced Oil Recovery, Research Institute of Petroleum Exploration and Development of PetroChina, Beijing 100083, China; wujiazhong@petrochina.com.cn (J.W.); yangsiyu@petrochina.com.cn (S.Y.)

⁴ Department of Chemistry and Chemical Engineering, Guangzhou University, Guangzhou 510006, China; ccyudanfeng@gzhu.edu.cn (D.Y.); xuwu@gzhu.edu.cn (X.W.)

⁵ Petroleum Engineering Technology Research Institute, Shengli Oilfield Branch, China Petrochemical Corporation LTD, Dongying 257000, China; maq7979@163.com (A.M.); skj502@sina.com (K.S.)

* Correspondence: yanghui@iccas.ac.cn; Tel.: +86-10-625-233-95; Fax: +86-10-625-233-95

Received: 23 June 2020; Accepted: 3 August 2020; Published: 7 August 2020



Abstract: Although stimuli-responsive release systems have attracted great attention in medical applications, there has been no attempt at “precise” deep profile control based on such systems, which is greatly need to improve oil recovery. With this in mind, we provided a facile and simple strategy to prepare stimuli-responsive composite capsules of amphiphilic dendrimers–poly(styrene sulfonic acid) sodium/halloysite nanotubes (HNTs) via layer-by-layer (LbL) self-assembly technique, controlling the release crosslinking agent methenamine under different pH or salinity conditions. The release time of methenamine encapsulated in multilayer shells is about 40 h, which can be prolonged with the introduction of salt or shortened via the addition of acid, which accordingly induces the gelation of polyacrylamide (PAM) solutions, taking from a few hours to a dozen days. This study provided a novel approach for controllable release of chemical agents and controllable crosslinking of deep profiles in many application fields.

Keywords: amphiphilic dendrimer; LbL assembly; dual-responsive nanocapsule; controllable release and gelation

1. Introduction

Stimuli-responsive delivery devices, known as “smart” release nanosystems, are poised to be used in diverse applications such as tumor therapy, antiseptis, and corrosion protection, which require tuning release via external stimuli [1–3]. Most recently, controllable release systems have been desired in practical application fields such as the petroleum industry due to the great need for “precise” profile control in order to enhance oil recovery [4–7]. After long-term water flooding, the vertical heterogeneity of a reservoir’s porosity is dramatically enlarged, resulting in increased water outflow and decreased crude oil production. Deep control seems to be a promising way to solve the problem by improving the efficiency of the water sweeping process into the middle-low permeability reservoir, thus enhancing oil recovery. The traditional method in profile control is that the mixing fluid, composed of polyacrylamide and a crosslinking agent, is injected without “precise” control of the gelation time, causing a blockage

near the bottom of the well and reducing the water flooding efficiency. The ideal gelation time should be able to be regulated over a wide range and selected according to the real oil field conditions, for which problems still remain due to unpredictable gelation positions [8]. Stimuli-responsive nanocapsules are proposed as a potential candidate system to realize precise deep control and improve the efficiency of oil production through controlling the releasing rate of the crosslinking agent and correspondingly regulating the gelation time and position [9]. The prepolymer is crosslinked with the crosslinking agent released by the nanocapsules when they reach the expected position, and the crosslinked polymer with increased viscosity moves forward with the injected water, blocking the flow channel of the high-permeability reservoir and changing the flow direction of the injected reservoir. The sweep coefficient of the injected water can be greatly improved, thus improving the oil recovery. Currently, such research and technology are still lacking, due to missing materials and insufficient understanding of the related stimuli-responsive mechanisms.

Amphiphilic dendrimers, as an important branch of the dendrimer family, can be endowed with amphiphilic balance and unique aggregation behavior by introducing appropriate modifications [10–15]. Compared with conventional dendrimers, amphiphilic ones show a talent for forming various self-assembled structures on solid surfaces, which may respond to external stimuli, such as the pH and ionic strength [16,17]. In our previous study, we designed a series of alkyl-terminated cationic poly(amidoamine) dendrimers with different generations, exhibiting flexible supramolecular self-assembly at different salinity levels [18,19]. It can be predicted that a smart nanocontainer based on such dendrimer systems may possess perfect environmentally sensitive functions. With this in mind, we have fabricated a series of responsive layer-by-layer (LbL) assemblies, which were assembled via electrostatic interaction between cationic amphiphilic dendrimers and anionic poly(styrene sulfonic acid) sodium (PSS) and which were used to modify halloysite nanotubes (HNTs) as cargo delivery in this study. The methenamine release behavior was shown to be ideal in such nanosystems, covering a wide range from a couple of hours to a dozen days at different salinity or pH values, while the polyacryamide (PAM) crosslinking performance was further carried out under control. In practical applications, the gelation time and strength can be manipulated precisely through adjusting the pH and salinity of the injected water according to the specific reservoir conditions. To the best of our knowledge, this is the first time this kind of dual-responsive nanocapsule system has been developed and the controllable release mechanism has been explored, which is expected to provide guidance and a reference for environmentally responsive, low-cost, environmentally friendly delivery systems in application fields.

2. Experimental Section

2.1. Materials

Halloysite nanotubes (HNTs) were purchased from the Guangzhou Runwo Materials Technology Co., Ltd. (Guangzhou, China), followed by fine grinding and purification according to previous reports [20–23]. Amphiphilic dendrimers G_nC_{12} ($n = 1, 2, 3$) were synthesized as shown in Scheme S1 and the detailed characterization results are exhibited in Figures S1–S3. NaCl solution was selected to explore the salinity responsiveness of LbL assemblies, because NaCl is a commonly used inorganic salt in injected water in oil fields. Poly(styrene sulfonic acid) sodium (PSS, $M_w \approx 70000$), NaCl, HCl, and methenamine were all purchased from Alfa Aesar (Ward Hill, MA, USA). Deionized water was used for all the experiments.

2.2. Methods

The adsorption and responsiveness of LbL assemblies onto solid surfaces were achieved using a Q-Sense E1 instrument (Biolin Scientific AB, Gothenburg, Sweden). Silica coated AT-cut quartz crystals (QSX 301, Biolin Scientific AB, Gothenburgcity, Sweden) with a resonant frequency of 4.95 MHz were selected to represent HNT surfaces, due to the similar amount of hydroxyl groups at the surface.

The quartz crystals were cleaned by plasma treatment using an O₂-plasma etcher for 15 min, followed by an immersion in 2 vol% sodium dodecyl sulfate in water for 10 min, rinsing with Milli-Q water, drying with nitrogen, and a final O₂-plasma treatment for 10 min. The temperature for all the quartz crystal microbalance with dissipation (QCM-D) experiments was 25 °C. The flow rate for all solutions was kept at 100 µL/min. The baseline for each measurement was established by flowing deionized water over the quartz crystal for approximately 1 h. Adsorption of LbL film was carried out by alternating the flow of G_nC₁₂ at 5 mg/mL and PSS at 5 mg/mL for 10 min each time. After each adsorption, the system was rinsed for 5 min with deionized water. All films in this study were capped or terminated with G_nC₁₂ and the total number of layer pairs was 5.5. After the final rinse, the films were exposed to either NaCl solution at different concentrations or deionized water at different pH values. Changes in frequency and dissipation from each QCM-D experiment were analyzed using QTools modeling software (Biolin Scientific AB, Gothenburg, Sweden). The surface topography was characterized using a FASTSCAN atomic force microscope (AFM, Bruker Instruments, Madison, WI, USA) in peak-force tapping mode using a silicon cantilever, with a nominal spring constant of 4 N/m and at a scan rate of 1.0 Hz. The cross-section analysis and the roughness (R_q) of adsorbed layers in air were evaluated by the Nanoscope Analysis software (Nanoscope Analysis 2.0, Bruker, Madison, WI, USA). HNTs were dispersed in aqueous solution at a concentration of 0.05 wt.%, which was dropped onto holey carbon film on copper grids, then the excess liquid was removed by filter paper. The morphology of the HNT samples was observed under JEM-1011 transmission electron microscopy (TEM, JEOL, Akishima, Japan) at 200 kV acceleration voltage. The ζ -potential values of different LbL systems were measured on a Nano-ZS instrument (Malvern Instruments Ltd., Malvern, UK). The compositions of HNTs samples were determined by a TENSOR-27 Fourier-transform infrared spectroscopy instrument (FTIR, Bruker, Karlsruhe, Germany), with spectra ranging from 4000 to 400 cm⁻¹, and the disk shaped samples were obtained by compression molding with KBr. The weight change of HNTs was examined by TG-DTA6300 thermogravimetric analysis (TGA, NSK, Tokyo, Japan) from 30 to 700 °C at a heating rate of 10 °C/min under a N₂ atmosphere. The percentage of modification of HNTs was calculated using the following equation: modification ratio (%) = (m_1/m_2) × 100%, where m_1 (g) is the weight of organics modified onto HNTs and m_2 (g) is the weight of HNTs. The colloidal viscosity of the PAM gel system was determined using a Bruker Rotary Viscometer (Bruker, Madison, WI, USA).

2.3. Fabrication of Methenamine-Loaded HNTs

To entrap methenamine, purified HNTs were mixed as dry powders with a saturated solution of methenamine in ethanol at 1.2 g/mL. A beaker containing methenamine and the HNT suspension was transferred to a vacuum jar, which was then evacuated using a vacuum pump. The methenamine solution was drawn into the internal cavity of HNTs in the presence of negative pressure for 1–2 h [24]. The whole process was repeated 3 times in order to increase the loading efficiency. The nanotubes were washed with distilled water separated by centrifugation. It was reasonable that the methenamine molecules were loaded into the interior cavity of HNTs through the hydrogen bond interactions between their tertiary amine groups and hydroxyl of HNTs.

2.4. LbL Assembly of G_nC₁₂/PSS Multilayers, Modifying the Methenamine-Loaded HNTs

LbL assemblies on HNTs were achieved via following the procedures: 0.1 g HNTs loaded with methenamine were first added into 20 mL G_nC₁₂ solution at 10 mg/mL and shaken at 200 rpm at room temperature for 10 min, followed by rinsing with deionized water and centrifuging 3 times. Then, the modified HNTs were dispersed into 20 mL PSS solution (10 mg/mL) for 10 min, followed by washing with deionized water and centrifuging 3 times. The same procedure was repeated 5.5 times to obtain the multilayer of HNT-(G_nC₁₂/PSS)_{5.5}.

2.5. Controllable Release of Methenamine

The release behavior of methenamine from the HNTs-(G_nC_{12}/PSS)_{5.5} systems was examined by measuring the amount of methenamine released into the bulk solution. Here, 50 mg methenamine-loaded HNT nanocapsules was put into a dialysis tube (MWCO = 2500 Da) and dialyzed against 100 mL distilled water at room temperature. Then, 2 mL solution was taken out from the dialysis solution at set intervals to measure the concentration of the released methenamine from the UV adsorption band at 215.5 nm according to the standard methenamine curve. At the same time, 2 mL distilled water was added to the mixed solution to keep the volume constant. The percentage of the total methenamine released from the nanocapsules was obtained and plotted as a function of time. The cumulative methenamine released was calculated according to Equation (1), in which M_t represents the methenamine amount released in time and M_∞ represents the total methenamine amount released.

$$\text{Cumulative methenamine release (\%)} = M_t/M_\infty \times 100\% \quad (1)$$

2.6. Crosslinking Evaluation

The crosslinking efficiency of HNTs-(G_nC_{12}/PSS)_{5.5} for the dilute PAM solution was performed by measuring the colloidal viscosity after adding HNTs-(G_nC_{12}/PSS)_{5.5} loaded with the crosslinking agent methenamine at different NaCl concentrations and pH values.

3. Results and Discussion

3.1. LbL Assembly and Responsiveness to Salt and pH

The constructing process of G_nC_{12}/PSS LbL thin films and the responsive performances in the external environment were investigated with the QCM-D method in situ. The (G_nC_{12}/PSS)_{5.5} films were assembled by alternately loading G_nC_{12} and PSS solutions onto SiO_2 -coated quartz crystals, as shown in Figure 1a–c. The final Δf values of the LbL films for G_1C_{12} , G_2C_{12} , and G_3C_{12} were around -90 Hz, -120 Hz, and -260 Hz, respectively, indicating a dependence on dendrimer generation, which is mainly caused by the increased molecular weight and more adsorbed dendrimer molecules due to the stronger hydrophobic interaction at higher generation [25]. The increase in ΔD with the higher generation indicates a softer film with more hydrophobic microdomains in the LbL films. In the same way, LbL nanoshells are fabricated by assembling alternating layers of G_nC_{12} and PSS onto HNTs, which is demonstrated by zeta potential measurements (Figure 1d–f). A reversal in charge after each adsorbed layer suggests that the corresponding components are sequentially deposited. Accordingly, the zeta potentials of the G_nC_{12} -adsorbed layer reach 25–40 mV due to its positive nature, but turn negative in the case of the PSS adsorbed layer.

The bare HNT sample had a cylindrical-shaped tubular morphology and open-ended lumen, with an average a diameter of 10–20 nm, as determined by TEM (Figure 2a). In comparison, the rough surface and capped tube ends demonstrated the existence of the LbL nanoshells on HNTs, as shown in Figure 2b–d. The LbL self-assembly of HNTs was also confirmed by FTIR analysis, in which the spectra of HNTs-(G_nC_{12}/PSS)_{5.5} displayed alkyl chain vibration band at around 2980 cm^{-1} (Figure 2e), which was not distinct because of the low ratio of dendrimers in the nanocomposites. Additionally, the peak areas at $3400\text{--}3700\text{ cm}^{-1}$ belong to O–H stretching vibration absorption of HNTs; the peak areas of $1000\text{--}1100\text{ cm}^{-1}$ belong to Si–O stretching vibration absorption of HNTs. TGA curves (Figure S4) reveal that the residual mass fractions of HNTs with LbL multilayers are lower than pristine HNTs and decrease with increasing dendrimer generations. The above results demonstrate the successful assembly of LbL multilayers on HNTs.

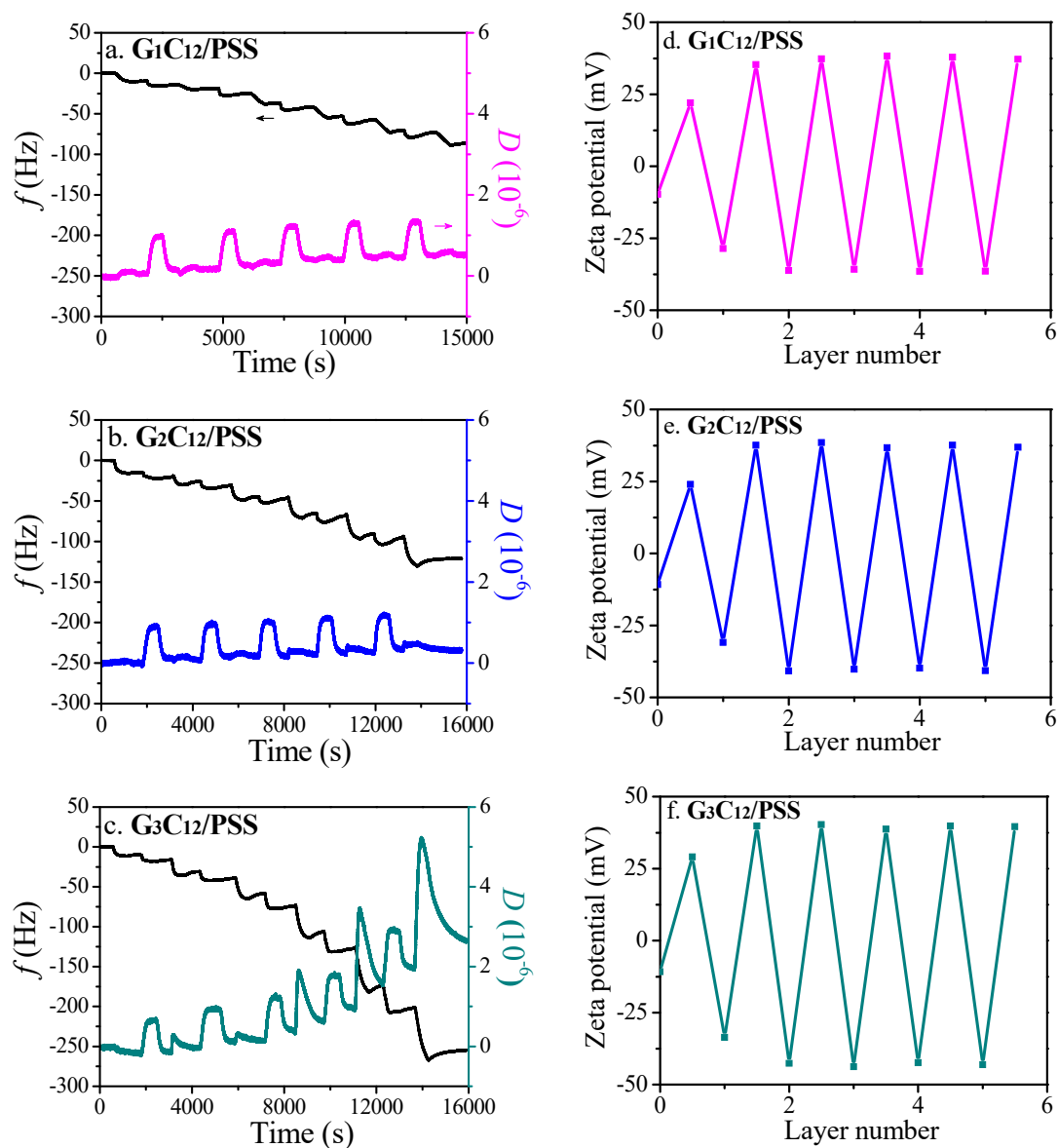


Figure 1. Shifts of frequency and dissipation as a function of time for multilayer assemblies of (a) G₁C₁₂/PSS, (b) G₂C₁₂/PSS, and (c) G₃C₁₂/PSS. Zeta-potentials as functions of the coating number on HNTs modified by (d) G₁C₁₂/PSS, (e) G₂C₁₂/PSS, and (f) G₃C₁₂/PSS multilayers.

After the assembly, the thin films with a roughness of ≈ 3 nm (Figure S5) were exposed to the NaCl solution at a given concentration under dynamic flow, then after rinsing the films were incubated in another brine at a higher ionic strength as a subsequent rinsing step. Figure 3a–c shows the decreasing Δf values and increasing ΔD values when the salt concentration increases from 50 mM to 1000 mM. Compared with the salt effect on the bare SiO₂ substrate (Figure S6), this indicates that the modified films become more viscoelastic and swell during the salt flushing process. This can be attributed to the adsorption of counterions into the interior of the LbL film, resulting in electrostatic screening on the ion pairs of G_nC₁₂ and PSS and concomitant film swelling [26,27]. A similar trend can be observed with higher dendrimer generation and with a higher amount of positively charged amino groups. Therefore, with either higher salt concentration or higher dendrimer generation, LbL films tend to swell more, which may result in a slower release of guest molecules.

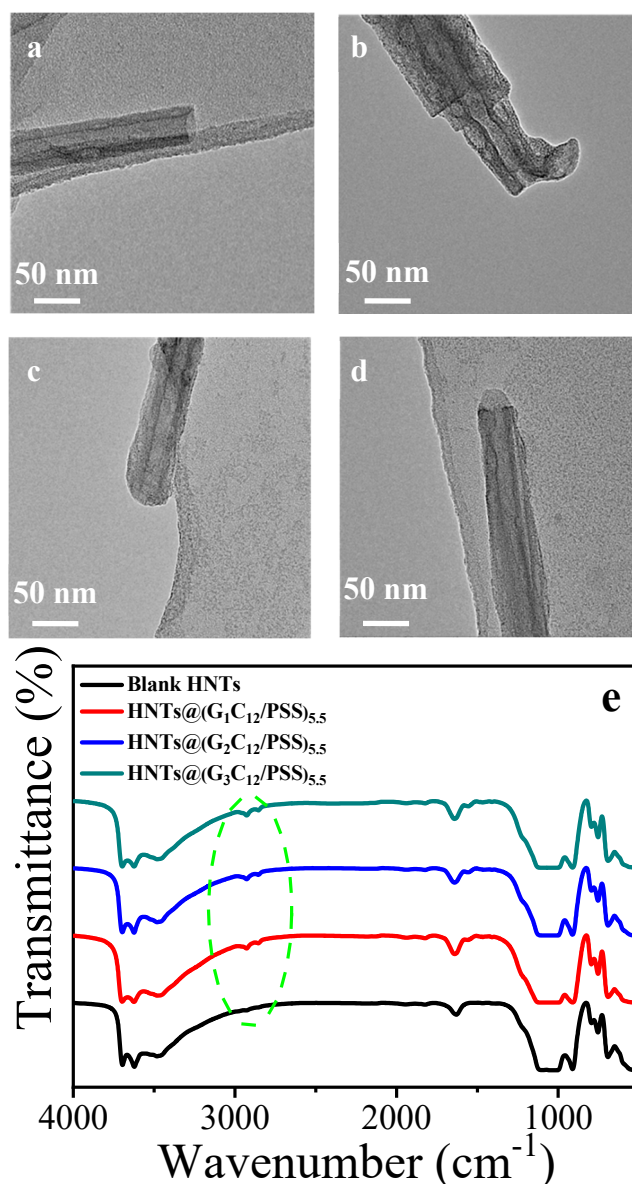


Figure 2. TEM images of (a) bare HNTs, (b) HNTs@(G₁C₁₂/PSS)_{5.5}, (c) HNTs@(G₂C₁₂/PSS)_{5.5}, (d) HNTs@(G₃C₁₂/PSS)_{5.5}. (e) FTIR spectra of bare HNTs, HNTs@(G₁C₁₂/PSS)_{5.5}, HNTs@(G₂C₁₂/PSS)_{5.5}, and HNTs@(G₃C₁₂/PSS)_{5.5}.

Interestingly, when lower pH values are introduced to the LbL films (Figure 3d–f), there is an increase in frequency and a decrease in dissipation, indicating a desorption of films, which agrees with the decreasing surface roughness at lower pH values (Figure S7) compared with those in a neutral environment (Figure S5). This can be attributed to the higher degree of the protonation of PSS [27,28] and the weaker electrostatic interactions of the PSS-dendrimer at lower pH values. With higher dendrimer generation, there is also a large reduction of electrostatic interactions between the PSS and dendrimer, resulting in higher desorption of films. Therefore, with either a higher acidic environment or higher dendrimer generation, LbL films tend to gradually detach from the substrate, which may result in a quicker release of guest molecules.

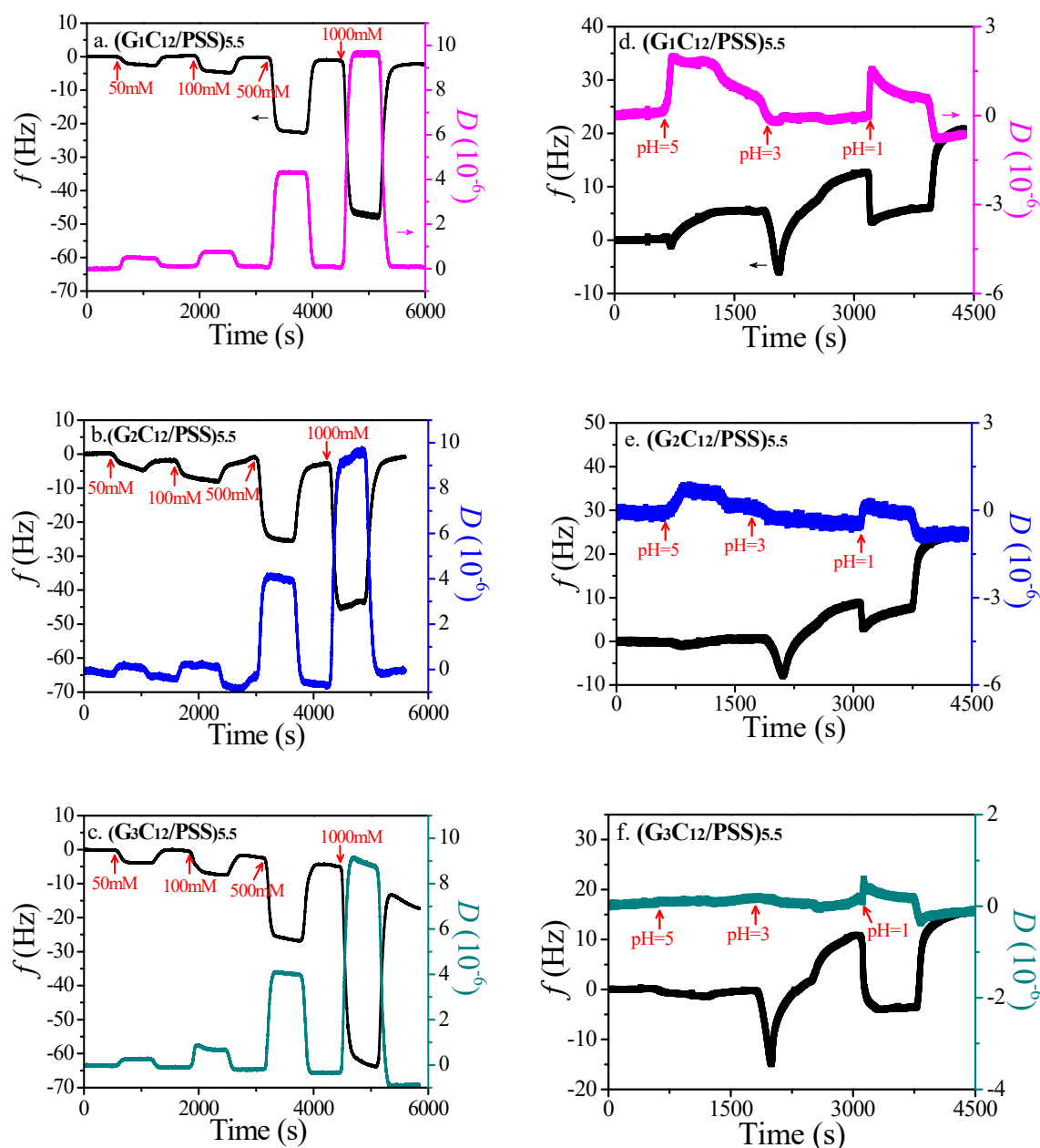


Figure 3. Shifts of frequency and dissipation in response to salt for multilayer assemblies of (a) $(G_1C_{12}/PSS)_{5.5}$, (b) $(G_2C_{12}/PSS)_{5.5}$, and (c) $(G_3C_{12}/PSS)_{5.5}$; and in response to pH for multilayer assemblies of (d) $(G_1C_{12}/PSS)_{5.5}$, (e) $(G_2C_{12}/PSS)_{5.5}$, and (f) $(G_3C_{12}/PSS)_{5.5}$.

3.2. Release Performance of the Loaded Methenamine

The dependence of methenamine release on the dendrimer generation, salinity, and pH condition was investigated to evaluate the performance of the salt and pH dual-responsive HNTs- $(G_nC_{12}/PSS)_{5.5}$ nanocomposites. Figure 4a displays the cumulative methenamine release from HNTs- $(G_nC_{12}/PSS)_{5.5}$ with different dendrimer generations in deionized water. The bare HNTs exhibit a rapid release of 80% in 2 h, whereas the encapsulation via LbL assemblies eliminates the burst release to 30–40 h. The guest molecules are released slowly with the higher dendrimer generation due to the formation of thicker nanoshells in such cases. As the salt concentration arises, the release rate is lower in the presence of HNTs- $(G_3C_{12}/PSS)_{5.5}$, as shown in Figure 4b. This can be explained by the fact that the influx of salt ions into the shell can shield the dendrimer–PSS ion pairs, inducing the film swelling and inhibiting the release of methenamine to some extent. At lower pH values, the release rate is higher, taking

HNTs-(G₁C₁₂/PSS)_{5,5} as an example (Figure 4c). This shows the pH-sensitive nature of LbL nanoshells, which cause the protonation of PSS and weaken the electrostatic attraction between the dendrimer and PSS, resulting in the gradual desorption of films and the quicker release of methenamine. The results demonstrate that the series of HNTs-(G_nC₁₂/PSS)_{5,5} nanocomposites can release cargoes in several hours and up to several days in response to salinity and pH stimuli, as illustrated in Figure 4d.

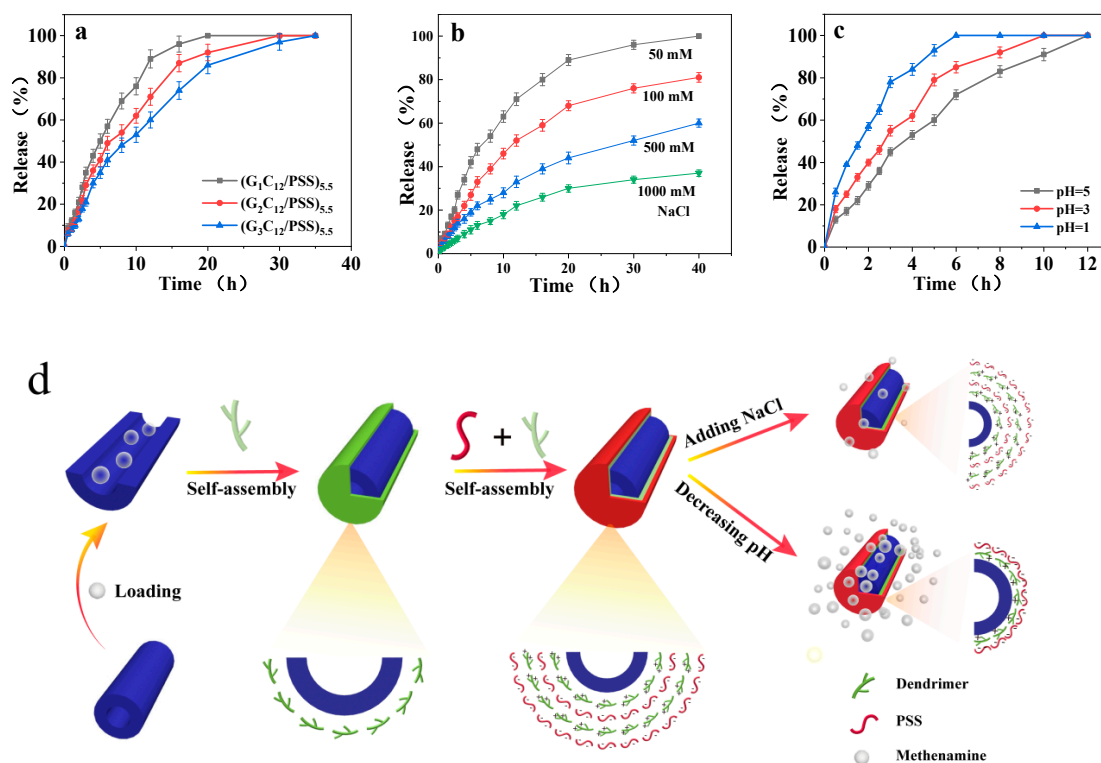


Figure 4. Release profiles of methenamine from different systems: (a) LbL assemblies in the presence of different dendrimer generations, (b) in the presence of NaCl at different concentrations in HNTs@(G₃C₁₂/PSS)_{5,5} systems, (c) under different pH values, and in the presence of HNTs@(G₁C₁₂/PSS)_{5,5}. (d) Schematic illustration of HNTs@(G_nC₁₂/PSS)_{5,5} with salinity–pH dual-responsive release performances.

3.3. Crosslinking Efficiency in PAM System

The practical crosslinking experiment was performed to evaluate the crosslinking efficiency of the hybrid controllable system loaded with methenamine into dilute PAM solutions. The colloidal viscosity of the PAM solution increases to a maximum value of 8000 mPa·s at 20 h in the presence of bare HNTs (Figure 5a), showing a gel state and a typical “tongue thrust” phenomenon (Figure 5c and Movie S1). For the methenamine loaded with the modified HNTs, the colloidal viscosity decreases notably compared with the bare HNTs, the maximum viscosity value of 4000 mPa·S reaches 40 h, and the system is not accompanied with the gel formation. The introduction of NaCl to the system dramatically decreases the crosslinking rate of the PAM solution, in which the colloidal viscosity is merely 1400 mPa·S and 800 mPa·S at salinity values of 100 mmol/L and 500 mmol/L after 60 h, respectively. Furthermore, the gel formation under 500 mmol/L NaCl occurs after about 15 days (Figure 5d and Movie S2) due to the decreasing release rate of methenamine triggered by salt. The lower pH in systems can speed up the gel formation (Figure 5b) compared with the pure HNTs-(G₁C₁₂/PSS)_{5,5} system, as indicated by the increased colloidal viscosity. The viscosity reaches 5500 mPa·S and 4000 mPa·S at pH = 5 and pH = 3, respectively, while the PAM gel forms at ≈3 days for pH = 5, as shown in Figure 5e and Movie S3. The release rate of methenamine is accelerated in lower pH conditions due to the desorption of films. From all the results above, a series of dual-responsive nanocapsules based on layer-by-layer

assemblies are fabricated, which is predicted to precisely control the release of crosslinking agents and the formation of gelation from a few hours to a dozen days.

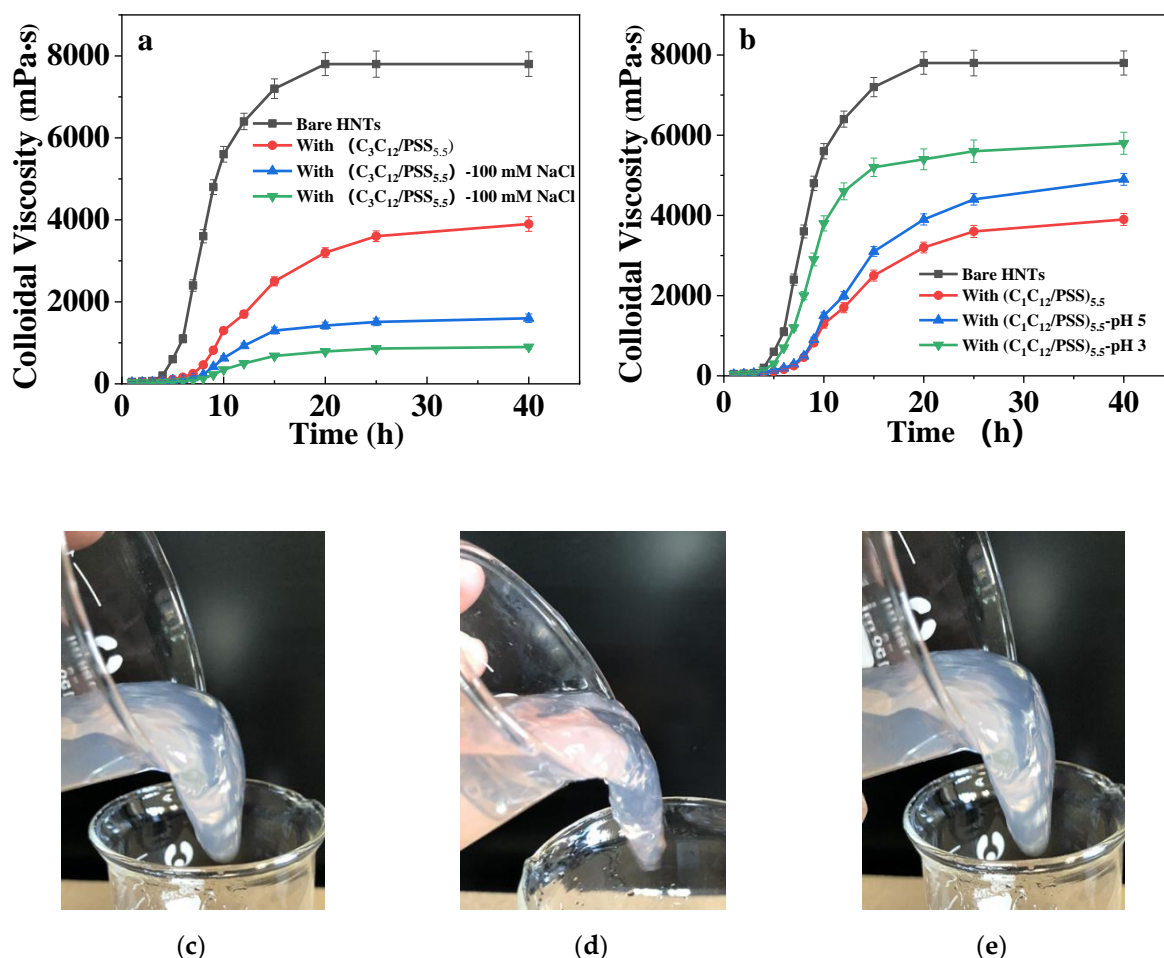


Figure 5. The colloidal viscosity–time profiles of polyacryamide solutions under different conditions: (a) in the presence of NaCl at different concentrations and HNTs@(G₃C₁₂/PSS)_{5.5}; (b) under different pH values and in the presence of HNTs@(G₁C₁₂/PSS)_{5.5}; (c) PAM gel without HNTs; (d) PAM gel in the presence of NaCl at different concentrations in HNTs@(G₃C₁₂/PSS)_{5.5} systems; (e) PAM gel at pH = 5 in the presence of HNTs@(G₁C₁₂/PSS)_{5.5}.

4. Conclusions

A series of salt- and pH-responsive controlled release systems, in which amphiphilic dendrimers and poly(styrene sulfonic acid) sodium polymers self-assemble on halloysite nanotubes via the LbL technique, which can control the release rate of methenamine and the crosslinking rate of PAM. Methenamine is released slowly at higher NaCl concentrations due to the swelling of dendrimer–PSS films because of the electrostatic shielding effect, and rapidly at lower pH values because of the desorption of the films, which is caused by the weakened interlayer interaction. Accordingly, the formation time of the PAM gel can be perfectly controlled from a few hours to a dozen days, providing a potential way to achieve “precise” profile control. In summary, a new type of dual-responsive nanocapsule has been developed to encapsulate guest molecules and control the release on demand, which is a candidate for diverse applications in environmentally dependent nanostructures.

Supplementary Materials: The following are available online at <http://www.mdpi.com/1996-1944/13/16/3479/s1>: Scheme S1: The synthesis pathway of amphiphilic dendrimer G₁C₁₂, Figure S1: Characterization data of G₁C₁₂ by ¹H NMR, Figure S2: Characterization data of G₂C₁₂ by ¹H NMR, Figure S3: Characterization data of G₃C₁₂ by ¹H NMR, Figure S4: TGA curves of pristine HNTs, HNTs@(G₁C₁₂/PSS)_{5.5}, HNTs@(G₂C₁₂/PSS)_{5.5}, and

HNTs@(G_3C_{12}/PSS)_{5.5} under N_2 , Figure S5: The $5\ \mu\text{m} \times 5\ \mu\text{m}$ AFM images: (a) (G_1C_{12}/PSS)_{5.5}; (b) (G_2C_{12}/PSS)_{5.5}; (c) (G_3C_{12}/PSS)_{5.5}, Figure S6: Shifts of frequency and dissipation for multilayers in response to different salt concentration as a function of time for bare silica substrate, Figure S7: The $5\ \mu\text{m} \times 5\ \mu\text{m}$ AFM images of adsorbed (G_1C_{12}/PSS)_{5.5} films in response to different pH buffer solutions: (a) pH = 5; (b) pH = 3; (c) pH = 1, Movie S1: PAM gel at pH = 5 in the presence of HNTs@(G_2C_{12}/PSS)_{5.5}, Movie S2: PAM gel in the presence of NaCl. Movie S3: PAM gel without HNTs.

Author Contributions: Conceptualization, H.Y. and J.W. (Jinben Wang); methodology, H.Y.; software, M.Z.; validation, S.Y., M.Z. and D.Y.; formal analysis, A.M.; investigation, M.Z.; resources, X.W.; data curation, X.W.; writing—original draft preparation, M.Z.; writing—review and editing, A.M. and K.S.; visualization, K.S.; supervision, J.W. (Jinben Wang); project administration, J.W. (Jiazhong Wu); funding acquisition, H.Y. All authors have read and agreed to the published version of the manuscript.

Funding: This work was funded by the National Natural Science Foundation of China (21872152 and 21603240), the Important National Science and Technology Specific Project of China (2017ZX05013-003 and 2016ZX05025-003-009), and the Strategic Priority Research Program of CAS (XDB22030102).

Acknowledgments: We thank Min Wang from Biolin Scientific AB for help with QCM measurements.

Conflicts of Interest: The authors declare no competing financial interest.

References

1. Wang, H.; Chen, Q.; Zhou, S. Carbon-Based Hybrid Nanogels: A Synergistic Nanoplatfrom for Combined Biosensing, Bioimaging, and Responsive Drug Delivery. *Chem. Soc. Rev.* **2018**, *47*, 4198–4232. [[CrossRef](#)]
2. Mai, B.T.; Fernandes, S.; Balakrishnan, P.B.; Pellegrino, T. Nanosystems Based on Magnetic Nanoparticles and Thermo- or pH-Responsive Polymers: An Update and Future Perspectives. *Acc. Chem. Res.* **2018**, *51*, 999–1013. [[CrossRef](#)] [[PubMed](#)]
3. Li, X.; Kim, J.; Yoon, J.; Chen, X. Cancer-Associated, Stimuli-Driven, Turn on Theranostics for Multimodality Imaging and Therapy. *Adv. Mater.* **2017**, *29*, 1606857. [[CrossRef](#)] [[PubMed](#)]
4. Li, Z.; Wang, S.; Tao, Y.; Ma, H.; Wu, J. Research and Application of the HTHS Anti- H_2S Gel Valve for Underbalanced Drilling. *J. Pet. Sci. Technol.* **2018**, *164*, 174–181. [[CrossRef](#)]
5. Chen, H.; Tang, H.; Wu, X.; Liu, Y.; Bai, J.; Zhao, F. Synthesis, Characterization, and Property Evaluation of a Hydrophobically Modified Polyacrylamide as Enhanced Oil Recovery Chemical. *J. Pet. Sci. Technol.* **2015**, *37*, 486–495. [[CrossRef](#)]
6. Alnazghah, M.; Kerans, C. Late Pennsylvanian Glaciation: Evidence of Icehouse Conditions from Canyon and Cisco Units, Midland Basin, Texas. *Mar. Pet. Geol.* **2018**, *94*, 198–211. [[CrossRef](#)]
7. Mao, J.; Wang, D.; Yang, X.; Zhang, Y.; Zhao, J.; Li, Y.; Zhao, J. Application and Optimization: Non-Aqueous Fracturing Fluid from Phosphate Ester Synthesized with Single Alcohol. *J. Pet. Sci. Technol.* **2016**, *147*, 356–360. [[CrossRef](#)]
8. Saghafi, H.R.; Naderifar, A.; Gerami, S.; Emadi, M.A. Improvement in Thermo-Chemical Stability of Nanocomposite Preformed Particle Gels for Conformance Control in Harsh Oil Reservoir Conditions. *Can. J. Chem. Eng.* **2016**, *94*, 1880–1890. [[CrossRef](#)]
9. Li, G.; Zheng, Z.; Möhwald, H.; Shchukin, D.G. Silica/Polymer Double-Walled Hybrid Nanotubes: Synthesis and Application as Stimuli-Responsive Nanocontainers in Self-Healing Coatings. *ACS Nano* **2013**, *7*, 2470–2478. [[CrossRef](#)]
10. Su, A.; Tan, S.; Thapa, F.P.B.N.; Ford, W.T. Highly Ordered Langmuir-Blodgett Films of Amphiphilic Poly(propylene imine) Dendrimers. *J. Phys. Chem. C* **2007**, *111*, 4695–4701. [[CrossRef](#)]
11. Ito, M.; Imae, T.; Aoi, K.; Tsutsumiuchi, K.; Noda, H.; Okada, M. In Situ Investigation of Adlayer Formation and Adsorption Kinetics of Amphiphilic Surface-Block Dendrimers on Solid Substrates. *Langmuir* **2002**, *18*, 9757–9764. [[CrossRef](#)]
12. Schenning, A.P.H.J.; Elissen-Roman, C.; Weener, J.-W.; Baars, M.W.P.L.; van der Gaast, S.J.; Meijer, E.W. Amphiphilic Dendrimers as Building Blocks in Supramolecular Assemblies. *J. Am. Chem. Soc.* **1998**, *120*, 8199–8208. [[CrossRef](#)]
13. Tan, S.; Su, A.; Ford, W.T. Aggregation of a Hydrophobically Modified Poly(propylene imine) Dendrimer. *Eur. Phys. J. E* **2008**, *27*, 205–211. [[CrossRef](#)] [[PubMed](#)]

14. Nummelin, S.; Selin, M.; Legrand, S.; Ropponen, J.; Seitsonen, J.; Nykanen, A.; Koivisto, J.; Hirvonen, J.; Kostianen, M.A.; Bimbo, L.M. Modular Synthesis of Self-Assembling Janus-Dendrimers and Facile Preparation of Drug-Loaded Dendrimersomes. *Nanoscale* **2017**, *9*, 7189–7198. [[CrossRef](#)] [[PubMed](#)]
15. Avila-Salas, F.; Pereira, A.; Rojas, M.A.; Saavedra-Torres, M.; Montecinos, R.; Bonardd, S.; Quezada, C.; Saldías, S.; Díaz, D.D.; Leiva, A.; et al. An Experimental and Theoretical Comparative Study of the Entrapment and Release of Dexamethasone from Micellar and Vesicular Aggregates of PAMAM-PCL Dendrimers. *Eur. Polym. J.* **2017**, *93*, 507–520. [[CrossRef](#)]
16. Pericet-Camara, R.; Cahill, B.P.; Papastavrou, G.; Borkovec, M. Nano-Patterning of Substrates by Adsorbed Dendrimers. *Chem. Commun.* **2007**, *3*, 266–268. [[CrossRef](#)]
17. Cahill, B.P.; Papastavrou, G.; Koper, G.J.M.; Borkovec, M. Adsorption of Poly (Amido Amine) (PAMAM) Dendrimers on Silica: Importance of Electrostatic Three-Body Attraction. *Langmuir* **2008**, *24*, 465–473. [[CrossRef](#)]
18. Zhang, P.; Zhang, L.; Zhou, L.J.; Wang, J.; Yan, H. Dilational Properties of Novel Amphiphilic Dendrimers at Water-Air and Water-Heptane Interfaces. *J. Phys. Chem. B* **2012**, *116*, 12760–12768. [[CrossRef](#)]
19. Zhang, M.; Wang, J.; Zhang, P. Controllable Self-Assembly of Amphiphilic Dendrimers on a Silica Surface: The Effect of Molecular Topological Structure and Salinity. *J. Phys. Chem. B* **2016**, *120*, 10990–10999. [[CrossRef](#)]
20. Hanif, M.; Jabbar, F.; Sharif, S.; Abbas, G.; Farooq, A.; Aziz, M. Halloysite Nanotubes as a New Drug-Delivery System: A Review. *Clay Miner.* **2018**, *51*, 469–477. [[CrossRef](#)]
21. Massaro, M.; Cavallaro, G.; Colletti, C.G.; D’Azzo, G.; Guernelli, S.; Lazzara, G.; Pieraccini, S.; Riela, S. Halloysite Nanotubes for Efficient Loading, Stabilization and Controlled Release of Insulin. *J. Colloid Interface Sci.* **2018**, *524*, 156–164. [[CrossRef](#)] [[PubMed](#)]
22. Cavallaro, G.; Danilushkina, A.A.; Evtugyn, V.G.; Lazzara, G.; Milioto, S.; Parisi, F.; Rozhina, E.V.; Fakhrullin, R.F. Halloysite Nanotubes: Controlled Access and Release by Smart Gates. *Nanomaterials* **2017**, *7*, 199. [[CrossRef](#)] [[PubMed](#)]
23. Liu, S.; Liu, J.; Pan, J.; Luo, J.; Niu, X.; Zhang, T.; Qiu, F. Two Are Better than One: Halloysite Nanotubes-Supported Surface Imprinted Nanoparticles Using Synergy of Metal Chelating and Low pKa Boronic Acid Monomers for Highly Specific Luteolin Binding under Neutral Condition. *ACS Appl. Mater. Interfaces* **2017**, *38*, 33191–33202. [[CrossRef](#)] [[PubMed](#)]
24. Zeng, X.; Zhong, B.; Jia, Z.; Zhang, Q.; Chen, Y.; Jia, D. Halloysite Nanotubes as Nanocarriers for Plant Herbicide and its Controlled Release in Biodegradable Polymers Composite Film. *Appl. Clay Sci.* **2019**, *171*, 20–28. [[CrossRef](#)]
25. Pan, Q.; Li, N.; Hong, Y.; Tang, H.; Zheng, Z.; Weng, S.; Zheng, Y.; Huang, L. Halloysite Clay Nanotubes as Effective Nanocarriers for the Adsorption and Loading of Vancomycin for Sustained Release. *RSC Adv.* **2017**, *7*, 21352–21359. [[CrossRef](#)]
26. O’Neal, J.T.; Dai, E.Y.; Zhang, Y.; Clark, K.B.; Wilcox, K.G.; George, I.M.; Ramasamy, N.E.; Enriquez, D.; Batys, P.; Sammalkorpi, M.; et al. QCM-D Investigation of Swelling Behavior of Layer-by-Layer Thin Films upon Exposure to Monovalent Ions. *Langmuir* **2018**, *34*, 999–1009. [[CrossRef](#)]
27. Benselfelt, T.; Pettersson, T.; Wågberg, L. Influence of Surface Charge Density and Morphology on the Formation of Polyelectrolyte Multilayers on Smooth Charged Cellulose Surfaces. *Langmuir* **2017**, *33*, 968–979. [[CrossRef](#)]
28. Zhang, Y.; Arugula, M.A.; Kirsch, J.S.; Yang, X.; Olsen, E.; Simonian, A.L. Layer-by-Layer Assembled Carbon Nanotube-Acetylcholinesterase/Biopolymer Renewable Interfaces: SPR and Electrochemical Characterization. *Langmuir* **2015**, *31*, 1462–1468. [[CrossRef](#)]

